A multi-method investigation of temperature, moisture and salt dynamics in tafoni (Tafraoute, Morocco)

Schnepfleitner H., Sass O., Fruhmann S.,Viles H. and Goudie A.

Department of Geography and Regional Science, University of Graz, NAWI Graz

School of Geography and the Environment, University of Oxford, OX1 3QY, Oxford, UK

Contact: harald.schnepfleitner@uni-graz.at

Earth Surface Processes and Landforms

Abstract

Despite numerous investigations and theoretical models, tafoni weathering is still not fully understood largely because of limited data available on temperature, moisture and salt regimes. We investigated tafoni developed in granite in the Tafraoute region, Morocco, through an exploratory, two-week multi-method field campaign. Temperatures were measured with iButtons and by means of infrared thermography; moisture distribution and progress were captured with handheld moisture sensors and with drilled-in iButtons. Salts were analysed in drill dust samples from different positions and rock depths.

The results derived from very different techniques mutually support one another. Salts and moisture are concentrated near the base of the investigated tafoni, probably due to a saturated pore water body around the base of rock tors. Salts are accumulated close to the rock surface in tafoni, but not on the surrounding rock surfaces. A clear correlation was found between moisture and salt contents. Within a

tafone, areas of higher humidity also display increased salt concentration near the surface. The temperature/humidity records allied with ionic analyses suggest that sodium sulfate dominates and is likely to undergo frequent phase changes from thenardite to mirabilite and vice versa. Two pathways of salt transport in and around tafoni are assumed based on the data: Infiltration with rainfall on the top and around tors and boulders, and capillary rise from saturated pore water bodies to the surface.

Keywords:

Tafoni, salt weathering, Morocco, rock moisture, ERT, Infrared, Salt concentration

Introduction

Cavernous weathering (tafoni formation) is a classic example of a feature most likely attributable to multifactorial processes. Tafoni (singular, tafone) occur in hot and arid conditions (Campbell, 1999), coastal environments (Mottershead and Pye, 1994), and even in Antarctica (Strini et al., 2008). Turkington & Paradise (2005) proposed detailed conceptual models of the evolution of tafoni in sandstones. They summarize the distribution as following: “[…] They occur under cold, temperate, hot, humid and arid environments, and are found on a variety of rock types." However, an arid period is generally considered necessary for tafoni development (Brandmeier et al., 2011). The governing processes might be physical or chemical or a combination of the two (French and Guglielmin, 2000; Dorn et al., 2013); various mechanisms like salt weathering, dissolution, alternating wetting and drying, temperature fluctuations and aeolian processes have been proposed (Mol & Viles, 2012). Tafoni development can only be explained by a complex combination of processes (Turkington & Phillips, 2004), although many authors believe salt weathering to be the most important single

process in many cases (Rodriguez-Navarro et al., 1999; Brandmeier et al., 2011) and moisture is often emphasized as a main driving factor (e.g. Mellor et al., 1997).

For understanding the development of tafoni, more data need to be collected on the environmental controls of the contributing weathering processes (e.g. salt weathering and hydration), in particular the temperature and moisture regimes and distribution of salts within tafoni and the surrounding rock. Our aim is to investigate the control parameters of tafoni formation in Tafraoute, Morocco, using an integrative approach which combines high-resolution temporal and spatial measurements of temperature, moisture and salt distribution. We aim to elucidate the small-scale interaction of temperature, rock moisture and salt levels and fluctuations that contribute to cavernous weathering in granite. Besides analyzing how, in the Tafraoute area, moisture and salts contribute to tafoni development the field data can be used to underpin (or challenge) theoretical and mathematical models of tafoni formation.

THEORIES AND CAUSES OF TAFONI WEATHERING

Temperature and moisture regimes and salt distributions have all been proposed as important drivers of tafoni development. The effectiveness of 'pure' insolation or temperature weathering has been discussed for decades and will not be reviewed here in detail. In recent years, authors such as Hall & André (2001) and Hall et al. (2007) have pointed out that insolation is an underrated process and introduced the terms thermal fatigue und thermal shock. Rapid temperature fluctuations of >2 K/min are regarded to be particularly important in causing rock breakdown, although the validity of this threshold has been recently challenged by Boelhouwers & Jonsson (2013). Nonetheless, there are still significant shortcomings in the availability of high-

70 resolution temperature data (Sumner et al., 2009). Temperature fluctuations in
71 isolation have never been considered as the main agent of tafoni formation; but they
72 might trigger moisture and salt movement. Two recent developments could contribute
73 to novel datasets of temperature fluctuations within and outside tafoni: (1) the use of
74 many cheap microsensors (iButtons) and (2) infrared thermography, which has, to
75 our knowledge, never been reported on in a published paper on tafoni.

76 Moisture content in porous rock outcrops is extremely variable in time and space;
77 quantitative assessment of moisture concentration is still challenging and there are
78 few results from field sites. Most earlier field results were derived from weighing and
79 drying samples (e.g. Hall, 1986, 1991). Matsukura & Takahashi (2000) measured
80 moisture of sandstone blocks using an infrared moisture meter, while Eklund et al.
81 (2010) tested and demonstrated the potential use of handheld capacitance and
82 resitance-based moisture meters. For one or two decades geophysical techniques,
83 such as 2D-geoelectrical measurements have been applied to natural rock (Sass,
84 2003, 2004; adapted by Mol & Viles, 2010) and the approach has been adapted to
85 building stone using non-invasive adhesive electrodes (Sass & Viles, 2010 a+b) for
86 monitoring moisture ingress into the stonework. Moisture distribution is commonly
87 regarded as one of the most important determinants of tafoni formation (Mellor et al.,
88 1997) and moisture gradients may be crucial for the concentration of salts in certain
89 topographic conditions (Huinink et al., 2004). The application of borehole humidity
90 sensors in the presented investigation is a novel approach that has not been used
91 before in this context.

92 Salts may derive from various sources (e.g. weathering of bedrock, road salts,
93 atmospheric aerosols, capillary rise from groundwater, and coastal spray) and exert
94 physical pressure on pore walls by thermal expansion, hydration, and crystallization

95 (Goudie and Viles, 1997). They are a particularly important agent of weathering in
96 arid, semiarid and urban environments and are considered highly important for tafoni
97 evolution (e.g. Rodriguez-Navarro et al., 1999). Salt weathering processes have
98 been reviewed by Doehne (2002) and intensively investigated in the context of
99 building stone deterioration and conservation (e.g. Maurício et al., 2006; Dionisio et
100 al., 2013). A variety of different salts is thought to be involved in stone decay
101 (Turkington et al., 2003). A very heterogeneous distribution of dissolved salts within
102 porous rock and stonework has to be considered in most environments. Capillary
103 uptake of groundwater and atmospheric humidity are the main pathways by which
104 salts enter rock and stonework (Martinho et al., 2012). Thus, uptake of moisture and
105 the behaviour of salt mixtures in the pores are mutually inter-connected (Tsui et al.,
106 2003; Franzen & Mirwald, 2009).

107

108 **STUDY SITES**

109 The Anti-Atlas in southern Morocco is a Cambrian mountain belt running from NE to
110 SW. Tectonic windows are found in this mountain belt in which Proterozoic rock
111 complexes crop out. One of these windows is the Kerdous Massif in the western Anti-
112 Atlas in which lies the Tasrirt Plateau at an altitude of 1000m (Soulaimani and Piqué,
113 2004). Our study site is located on this plateau south of the small town of Tafraoute
114 (GPS: 30°09’70’’N; 09°13’15’’W). The predominant rock in the area is the Tafraoute
115 Granite.

116

117 Figure 1: Overview of the study area. a: location; b: simplified geological map (taken
118 from Service Géologique du Maroc,1985); c: location of the investigated sites in the
119 study area; d: impression of the granite landscape (taken from site 1 looking north).

120 In the field, the 550 million years old Tafraoute Granite is reddish-brown and rather
121 coarse. Feldspar crystals of mm to cm in size can be quite easily removed from the
122 rough surfaces, and the rather low resistance towards drilling (we drilled up to 50 cm
123 deep with comparetively low effort) demonstrates that the rock is highly weathered in
124 its entirety. This is confirmed by our own laboratory measurements: While typical
125 textbook values for density of granite are between 2600 and 2800 kg m^{-3} and 0.4 to
126 1.5% for porosity (Materialarchiv, 2014), samples from the area showed a density of
127 2240 kg m^{-3} and a porosity of 8%. Details of the structural, geochronological and
128 geochemical data on Tafraoute Granite can be found in Hassenforder (1985, 1987),
129 Barbey et al. (2004) and Benziane (2007). In the granite landscape within an area of
130 approximately 100 km², countless tafoni with different characteristics in terms of their
131 shape, size and exposure occur especially on a number of tor-like outcrops. Pilot
132 survey mapping revealed no specific distribution in terms of aspect or elevation. We
133 chose six sites with tafoni of different size and shape which are shown in Fig. 2.

134

135 Figure 2: Representation of the different study sites; the black bar equates 2m

136 Due to logistical constraints we focused most data collection on site 1 and in
137 particular on the west-facing tafoni at this site. Due to the completeness of the
138 dataset obtained here, most of the presented results are derived from this site.
139 Selected results from other sites are mentioned either to underpin the results of site 1
140 or to demonstrate deviations between the sites.

141 There is no meteorological station directly in Tafraoute and so the climate parameters
142 had to be estimated from different internet sources (Fig. 3). As none of these sources
143 give precise details on the origin of the data we only calculated the mean value for
144 temperature and precipitation. Based on this calculation, Tafraoute has a mean

annual air temperature of approx. 16°C. Precipitation is c. 250 mm/yr with a pronounced winter maximum (= BSk climate according to Köppen-Geiger). Frost may occur occasionally in winter nights. These figures broadly correspond to large-scale climate maps of Morocco. During the period of investigation (April 2014), air temperatures (measured with an iButton under an improvised radiation shield) ranged between 22,5 and 9°C.

Figure 3: Climate in Tafraoute as derived from different internet sources (http://www.weatherbase.com/, http://www.worldweatheronline.com, http://en.climate-data.org)

METHODOLOGY

Fieldwork was carried out in February 2014 (during cool conditions in late winter). The investigations focused on the assumed basic influential parameters to tafoni formation: temperature, moisture and salts. The range of techniques we used to investigate these three parameters and the measurements actually carried out at the six sites are compiled in **Error! Reference source not found.**.

Table 1: Summary of measurements performed at the sites of investigation. Bold numbers: measurements presented in this paper. *: only two profiles displayed, **: only one profile displayed, at Site1E were also measured in 25cm for a short period (20/2/2014 – 24/2/2014)

INFRARED THERMOGRAPHY

We used a VarioCam HR infrared camera with a thermal resolution of 0.03 K, an accuracy of ±1.5°C and a spectral range from 7.5 to 14 µm. The detector size is 640x480 pixels and can be increased to 1280x960 pixels by resolution enhancement technology. The spatial resolution at 5 m distance is 3 mm. For the basics of infrared thermography we refer to G. Gaussorgues (1993); Schuster and Kolobrodov (2000); Budzier and Gerlach (2010) and others. Applications of IR Thermography to studies of rock walls are described by Teza et al. (2011). Emissivity is a key variable for thermography measurements and thus was determined in the field. To determine emissivity, one iButton measured air temperature and relative humidity and a second one the temperature of the rockwall within the sensor field of the IR camera. The air temperature data was then used to correct the evaluation software of the thermal images and the thermography data compared to the measurements from iButton on the rock wall. The difference was compensated for by modifying the emissivity factor. Various measurements showed very similar results with a calculated emissivity value of 0.95. Similar results have been published by Gruner (2004), Shannon et al. (2005) and Testo (2006).

Surface temperatures were measured on three consecutive days for 24 hours using a measurement interval of 10 min across the entire surface of three sides of the site 1 rock tor (E, W and S-facing). The aim of using this method was to derive daily average values of different micro-sites, temperature fluctuations and the possible

187 impact on moisture transfer processes. The parameters were modified according to
188 the mentioned emissivity of 0.95.

189

190 **MOISTURE METER**

191 A handheld moisture meter (Voltcraft MF-100) was used to determine the moisture in
192 the near-surface area both within and adjacent to selected tafoni. The capacitance
193 sensor is commonly used for detecting water damage in buildings; its electrical field
194 penetrates some 2 – 4 cm into the rock. The sensor can be used in geomorphology
195 to assess semi-quantitative moisture distributions on reasonably smooth and sound
196 surfaces (e.g. Eklund et al., 2013). Detailed descriptions on the technical background
197 can be found in James (1963) and Skaar (1988). The measurement points were
198 arranged in form of a grid with a mesh size of 25 cm at the respective sites; the total
199 area of the grid depended on the micro-topographic conditions at each site (usually
200 10 x 10 measurements). The experimental design was to measure pairs of grids –
201 one inside and one outside each tafoni, but lack of smooth and round surfaces
202 outside sometimes precluded this. To reduce uncertainties, each point was measured
203 three times. The final value was the mean of the three measurements. The aim was
204 to get an overview of relative moisture distribution across the near-surface zone.

205 **I-BUTTONS**

206 Miniature loggers (iButton Hygrochron™ DS1923) with 17,35mm diameter were used
207 to measure temperature and relative humidity (accuracy of 0.5°C and 0.5%). At site
208 1, two sensors were attached to the surface inside the tafoni (one in the upper third,
209 one in the lower third) and a reference sensor was positioned on the outside rock
210 wall. Additionally, the temperature conditions inside of the rock were determined by

211 Thermochron DS1922L iButtons inserted into 3, 25, and 50cm deep bore holes, each
212 18 mm diameter. Humidity was only measured at 3 cm and 50 cm with the exception
213 of site 1 (east) where moisture was also determined at 25 cm depth for a period of
214 four days (20/02/14 to 24/02/14). The Hygrochron buttons measure air humidity
215 through a small hole at the top of the metallic housing. For that reason, a second
216 borehole (6 mm in diameter and 5-8 mm longer) was drilled into the lower end of
217 each hole (see Figure 4). This was to provide a confined air space to measure
218 borehole humidity, in equilibrium with the surrounding rock moisture. The principle is
219 based on the sorption isotherm (e.g. Franzen and Mirwald, 2009), the line of
220 equilibrium moisture between air and rock in porous bodies at a certain temperature
221 (see also Krus, 1995 and Plagge et al., 2006). The iButtons were glued to a wooden
222 rod to insert them into the boreholes and the narrow space between rod and rock
223 was sealed at the surface with silicone paste. In fact, the rods fit so tightly into the
224 drillholes that one of them could not be recovered and we thus assume that humidity
225 transport along the rod is negligible. A similar setup of one Thermochron (25 cm
226 depth) and two Hygrochrons at 3 cm and 50 cm depth was also installed at three
227 further sites (additional to the four different orientations at site 1). Measurements
228 were recorded at intervals of three minutes over the period between 14/02/14 and
229 24/02/14. Data loss occurred due to vandalism and theft, therefore, no data exist for
230 some of the sensors from 19/02/14 to 21/02/14. At the main site 1 (west), seven days
231 of continuous measurement are available (14/02 - 19/02 and 21/02 - 24/02). Rock
232 moisture values were calculated from the humidity data based on the sorption
233 isotherm (Fig. 5), which was determined in a climate chamber.

234

Figure 4: Setup for temperature and relative humidity measurements at different depths. Hatching: wooden rod, gray: iButton.

Figure 5: Soption isotherm of the Tafraoute granite as derived from lab measurements

ERT

Electrical resistivity tomography (ERT) is a widely used geophysical tool for subsurface surveys and has been adapted for small-scale investigations on rock walls and building stone facades over the last decade (e.g. Sass, 2005; Mol & Viles, 2012). ERT is a geophysical profiling technique which detects zones of different electrical conductivity, usually along 2D-sections (for the principles we refer e.g. to Schrott and Sass, 2008). In the environment of weathered rock, different electrical properties are generally caused by heterogeneous water content and/or salt concentration. However, without the aid of further techniques, it is currently not possible to differentiate whether zones of high resistivity are caused by high water content, by soluble salts, or by a combination of both. We used a Geotom device equipped with 50 electrodes. On the relatively smooth surfaces within the tafoni, self-adhesive medical ECG-electrodes were used to establish electrical contact to the rock. Outside of the tafoni the surfaces were generally rougher and more friable and adhesive electrodes did not work properly; thus, we used metal screws temporarily inserted in small boreholes. On the backwall of the large west-facing tafoni at site 1, two profiles were measured: A vertical one from the bottom to the roof and a horizontal one about half way up. Electrode spacing was 6 cm resulting in total profile lengths of 2.94 m. Both profiles were measured every six hours over a 24-hour

period (19/2/14 – 20/2/14). ERT profiles of similar configuration were measured at most of the other sites as well, but solely single measurements without 24-hr monitoring.

2D-resistivity sections were calculated using the software package Res2Dinv (Geotomo Software, Penang, Malaysia). We tested the standard least-square inversion as well as robust inversion and compared both in order to verify the shape of detected anomalies. The measurement setups used were Wenner and dipole-dipole (e.g. Keary et al., 2002) which allow good resolution of surface-parallel layers (Wenner) and of lateral inhomogeneities (Dipole-Dipole), respectively. Both arrays were combined in Res2Dinv to benefit from the advantages of both measurements. We checked the results of the calculation with the depth of investigation (DOI) method (Oldenburg and Li, 1999; Marescot et al., 2003). The DOI is an empirical method for determining the depth down to which the results are considered trustworthy, and model regions with DOI index values >0.2 are usually considered unreliable in terms of their modelled absolute resistivity values (Hilbich et al., 2009; Angelopoulos et al., 2013).

DRILLING AND SALT SAMPLING

Sampling for salts was carried out by incrementally collecting the ample drilling dust from the installation of the iButtons and of further drillholes. This approach made it possible to sample at a range of depths and thus, to assess the concentration and the types of salts at different depths. At site 1, four drill holes were sampled; three inside the west-facing tafone (top, mid, bottom) and one from the open rock face beside the tafone. The samples were taken from the following six depth increments: 0-2.5 / 2.5-5 / 5-10 / 10-15 / 15-20 / 20-25 cm. Analyses were performed in the

283 Oxford Rock Breakdown Laboratory with the Ion Chromatography System Dionex IC
284 DX500.

285 In addition to ion chromatography, a simple conductivity measurement was
286 performed for each sample (1 g of drill dust dissolved in 5 ml of deionized water). The
287 aim of this was to provide a quick assessment of overall salt concentration. The
288 applied instrument was a Bench-Top conductivity meter (HI2315).

289 # RESULTS

290 The presentation of the results focuses on the west-facing tafone at site 1 (shown in
291 Figure 2) because of the completeness of the datasets collected there. All of the
292 following results refer to the inside of this tafone if not specified otherwise.

293 ## INFRARED THERMOGRAPHY

294 Data were collected every 10 min over an extended period (24 hours), each
295 measurement covering several m^2 with a spatial resolution of 3 mm. In Fig. 6a, the
296 result of the averaging of all measurements is shown. It is obvious that the inside of
297 the tafone is warmer on average than the surrounding rock surface. Furthermore, a
298 significant temperature difference occurs between the bottom and the top of the
299 tafone, whereas the surrounding rock surface shows more homogenous conditions.
300 Fig. 6b shows a horizontal and a vertical profile (along the lines indicated in Fig. 6a)
301 to illustrate this point. While there is almost no temperature difference in the
302 horizontal-profile (blue line), a significant temperature decrease towards the bottom
303 can be detected in the vertical profile (red line). The temperature difference is almost
304 3°C.

Figure 6: Results of the Infrared measurments. a: Average of the 24h-measurement (dots mark the positions for which the temperature fluctuations were analysed); b: Horizontal and vertical temperature profile (24-hr mean); c: daily temperature cycle at defined points; d: averaged temperature cycles for certain areas (see text).

In Fig. 6c the diurnal temperature cycles at defined positions (as marked in Fig. 6a) are displayed. The selected positions can be divided into three areas: Area one includes positions 1 to 8 (outside of the tafone, green lines), area two includes positions 9 to 15 (upper inside area of the tafone, red lines) and area three includes positions 16 to 24 (lower inside area of the tafone, blue lines). The respective mean values for each area were calculated (Fig. 6d). Area one (outside the tafone) shows the biggest amplitude and therefore the lowest (~3 °C) and the highest (~20 °C) values during the day. In the curves of areas two and three the maximum and minimum temperatures are subdued. Interestingly, the two curves run almost parallel to each other with the lower tafone being constantly cooler than the upper tafone. This effect cannot be caused by stronger emission at night (otherwise, the amplitudes would be higher); the most probable explanation is higher moisture content towards the base (see discussion). On the east side of site 1 the tafoni are much shallower and further away from the ground; accordingly, similar patterns were not recorded at this site (not displayed).

MOISTURE METER

As pointed out in the methodology section, this method can only be used to infer relative moisture distributions within the near-surface zone (0 – 4 cm) as the reliability for quantitative results is rather low (see e.g. Eklund et al., 2012). At the east-facing side of site 1, it was found that small, decimeter-scale tafoni are consistently wetter

than the unweathered surrounding rock (Fig. 7c). On the backwall of the large west-facing tafone at site 1, a distinct trend was found with a clear decrease of the relative moisture values towards the top (Fig. 7a). Thus, the lower area of the tafone seems to be moister than upper part, which corresponds to the findings of the infrared monitoring. Similar patterns were found at site 3 (Fig. 7d) even if the decrease of moisture with elevation is smaller at this site. Outside tafoni the rock was generally much drier and no differences in vertical direction were found (Fig. 7b).

Figure 7: Results of the moisture meter measurements. a: site 1 (west), inside the tafone; b: site 1 (west), outside of the tafone; c: site 1 (east), yellow-green patches correspond to small, shallow tafone; d: inside the tafone at site 3. Relative readings from 0 (dry) to 100 (wet); the black bar equates 2m

I-BUTTONS

Similar to the IR results, the iButtons show a reasonably constant temperature difference between top and the bottom of the tafone and the biggest amplitudes outside of the tafone (site 1, west-facing). The humidity data show a reverse diurnal variation with consistently higher relative humidity values at the bottom in comparison to the top (Fig. 8c). The reason for this is the difference in temperature, as cooler air can absorb less moisture. Thus, for understanding the process of water vapor diffusion relative humidity data are of limited benefit. The more significant water vapour pressure was computed from the temperature and relative humidity according to the Magnus formula (Defant and Defant, 1958). In terms of absolute vapour pressure it becomes clear that there are no humidity differences close to the surface inside (top or bottom) or outside the tafone (Fig. 8a).

A pronounced diurnal cycle of temperature was detected only at depths of 3 and 20 cm while variations at 50 cm were just about 0.5 °C per day (Fig. 8e). Similarly, there is a clear diurnal cycle in both relative humidity and absolute vapour pressure at 3 cm depth while both parameters are constantly high at 50 cm depth.

Figure 8: Results of iButtons measurement of Site1 (west)

Special attention was paid to the increase of vapour pressure with depth because vapour pressure differences trigger vapour diffusion. Between 50 and 3 cm, and from 3 cm to the surface, a vapour pressure gradient from the inner parts towards the surface was detected over the whole measurement period. Both curves depend on the time of the day: In the afternoon, the highest vapor deficit is located between 3 cm and the surface while in the morning hours, the maximum is between 50 cm and 3 cm, but there is no reversal at any time. This finding confirms that moisture is constantly transported from the interior to the surface, even if the transport in the gaseous phase is not able to move salts through the rock.

Relative humidity values from the iButtons can be converted into degree of (liquid) pore saturation via the laboratory-measured sorption isotherm (Figure 5). The average pore saturation in our measurement period was ~80 % at 50 cm depth and ~10 % at 3 cm.

ERT

Figure 9 displays the vertical and horizontal profiles at site 1, site 3 and site 4 (Wenner and Dipole-Dipole measurements were combined in all cases). All extend to

a depth of about 30 cm to 40 cm inside the rock. The limits of resistivity for granite vary, depending on the textbook literature, between 10^3 and 10^5 Ohmm (lower values for wet and higher values for dry rock). A similar range of values is found in all displayed profiles; the rather high maximal resistivity values can probably be attributed to the unusually high porosity (8%) of the Tafraoute granite. Because the structure of the rock appears to be homogeneous and fractures are absent, it is likely that the measurements represent areas of different moisture and/or salt contents. Two general patterns can be seen in the vertical profiles (Fig. 9 a+b): (1) Lower resistivity in the lower half of the profiles. For example, in the vertical profile of site 1, high values (>10^5 Ohmm) are found in the upper area and relatively low values (<10^3 Ohmm) near the bottom (Fig. 9a). As these resistivity patterns correspond well with the infrared and the moisure meter results, we assume that these low-resistivity zones represent wetter areas, possibly amplified by salts near the surface. (2) Higher resistivity deeper inside the rock, particularly in the upper half of the profiles. This contradicts the very clear results of the iButtons which indicate wetter conditions at depth. Thus, it is probable that the high conductivity/low resistivity recorded near the surface using ERT results from higher salt concentration not higher moisture levels.

Figure 9: Results of ERT measurement of Site1 west (a, c), Site3 (b) and Site4 (d). Each profile is combined from Wenner and Dipole-Dipole measurements; unit electrode spacing is 6cm.

Although the contrasts are smaller in the horizontal profile from site 1 (Fig. 9c), it is evident that the edge of the tafone is slightly drier than the middle, and that there is a slight increase in moisture towards the inside of the rock. Similar patterns were also found in the horizontal profile at site 4 (Fig. 9d) even if the resistivities are much

lower. All measurements have a rather low RMS (root mean square; for the exact values see figure 9) error and the DOI values (not displayed) do not exceed the threshold of 0.2 which indicates that the results reflect the real situation very well.

DRILLING AND SAMPLING

Figure 10 displays the salt concentrations found in the samples of the four drill holes at site 1. Large quantities of sodium and sulfate are apparent particularly near the surface, along with other ions. At all measurement sites, except for the outer drill hole, salt concentrations increase towards the surface. Certain general patterns can be detected: First, a greater amount of salts are found close to the surface at all three sites within the tafone; second, concentrations of sulfate and sodium (to a lesser degree of chloride, bromide and magnesium) increase from the top towards the bottom of the tafone; and third, the increase of salt concentrations near the surface is not found in the outer drill hole (Fig. 10a-d). These general findings are confirmed by the results of the drill dust conductivity measurements where maximum values are located at the surface and in the lower/moister area of the tafone (Fig. 11). Similar patterns were also found within the tafoni borehole at site 4, but in the case the drill profile outside of the tafoni on the top of the boulder (which was vertical and not horizontal) is noticeably different as there is a significant increase of the values with increasing depth.

Figure 10: Concentrations of major ions in rock powder from different depths collected from the drillholes of site 1 (west)

Figure 11: Conductivity values from rock powder from different depths collected from the drillholes in site 1 and site 3

Because of the very similar distribution of sodium and sulfate it can be assumed with high probability that the dominant salt is sodium sulfate (as thenardite, the heptahydrite form or mirabilite; see Fig. 13). According to Goudie (1977) and Goudie and Viles (1997), this salt is one of the most important agents of salt weathering especially in arid environments because of its high solubility in water, its ability to hydrate at humidities and temperatures frequently encountered in nature, and its long crystal habit.

DISCUSSION

Utility of the techniques applied

The applied multi-method approach, combining relatively simple methods (drill dust sampling, hand held moisture meters) with novel and more sophisticated techniques (borehole humidity and temperature, ERT, thermography) has been demonstrated to provide useful data with which to gain insight into temperature, moisture and salt distribution. The data complement and support each other. Based on the measured data the following results can be summarized:

- Temperature amplitudes are subdued within tafoni compared to those on the surrounding rock faces (derived from: *Infrared, iButtons*)
- Areas of elevated moisture content are found in the lower areas of the tafoni (*ERT, Infrared, iButtons, moisture meter*); the rock inside the tafoni is moister than that outside (*moisture meter*). The humidity/absolute water vapour pressure increases with increasing rock depth (*iButtons*).
- Inside, but not outside, tafoni there is an accumulation of salts close to the rock surface (*drill dust sampling*). Salt concentrations increase towards the base inside tafoni (*drill dust sampling*).

Drill dust sampling turned out to be particularly helpful to clarify the salt concentration along depth profiles. This simple technique has rarely been carried out before (Viles and Goudie, 1992). Due to the high amount of material collected for analysis at each depth interval (drill diameter 18 mm) the results are likely to be highly representative. In many studies, only small amounts of weathered material from the surfaces within tafoni was collected (e.g. McBride et al., 2000; Mustoe, 1983). The drilling results were well worth the logistic effort because they give very clear evidence of the vertical and depth distribution of salts. Of course this method is not an option in many protected areas or conservation sites. The information can be used to cross-check the ERT results: In the current example it shows that high salt contents are a factor affecting conductivity/ resistivity values only close to the surface (where counteracted by insufficient moisture) while resistivity patterns in the deeper subsurface must be caused by varying pore water content alone, as the salt levels are consistently low.

The measurements of borehole humidity have not been carried out before to our knowledge in comparable settings and they also delivered novel results, proving clearly that rock moisture (at the time of our measurements) increases with depth. As with drill dust sampling, the method depends on the availability of a battery-driven hammer drill and is likely to be more problematic on harder, less weathered granites. A longer measurement programme (months or years rather than dayes) would have been desirable and is planned for the future; it was not possible in the current field campaign for logistical reasons and because of vandalism. The cheap and easy-to-use hand held moisture meters were helpful to underpin the results of the ERT and IR measurements from which we infer spatial moisture distributions. However, the scatter of the measurements is very high and they are sometimes hardly

476 reproducible; accordingly, anything more than a very rough, semi-quantitative
477 orientation is not possible.

478 Finally, IR thermography (24 hr monitoring) proved to be very helpful to gain high-
479 resolution information on spatial and temporal patterning of surface temperatures and
480 to delimit moister and drier areas. The consistent temperature difference between the
481 upper and lower area within the west-facing tafone at site 1 clearly points to
482 evaporative cooling and thus, to higher amounts of moisture towards the base. This
483 process seems to be so strong that even the influence of direct radiation (west-
484 facing, approx. from 16:00 to 17:30) is suppressed. An effect of higher emission at
485 night can be ruled out because of the constant temperature difference throughout the
486 24 hr period. As these assumptions are clearly confirmed by the results of other
487 methods, IR thermography was shown to be a valid method to gain data on
488 temperature and moisture distribution. However, short measurement times (or single
489 shot images) are of very limited value.

490

491 *Origin and distribution of salts*

492 The results of our measurements show that moister areas near the surface also have
493 a higher salt content, a correlation found in many publications on tafoni (e.g. Bradley
494 et al., 1978). The reason is that moisture is the agent of transport for dissolved salts.
495 Possible sources of water that merit consideration include dew, fog, rain and
496 groundwater, and two processes are responsible for the movement of moisture in the
497 rock: capillary transport (which is also the main process of salt transport), and vapor
498 diffusion which is responsible for the dehydration of rock. As dehydration is, in turn,

499 responsible for the crystallization of salts the process of vapor diffusion has a great
500 influence on the position of salts in the rock.

501 Huinink et al. (2004) tried to simulate water and salt movement within a developing
502 tafone in a mathematical model. They regarded two different cases: a short drying
503 period and a long one (t=2000Δt) and their results show that a long drying period is
504 very important for the development of tafoni because there is ample time for salts to
505 migrate to the slow-drying areas, following gradients of concentration. This
506 mechanism is also held responsible for the tendency of tafoni to grow upward
507 because *"most salt accumulates at the more sheltered (from the sun) part of the rock*
508 *surface, having the lowest drying rates, given that the drying period in a*
509 *wetting/drying cycle is long enough. Therefore, these parts weather faster than the*
510 *exterior part and cavernous structures, e.g. Tafoni, develop."* (Huinink et al. 2004,
511 p.1231). This mechanism explains the tendency of tafoni to grow upward. From our
512 own data (e.g. moisture meter) we are able to confirm that the interiors of tafoni dry
513 more slowly than external rock faces and that salts are concentrated in these regions
514 of slow drying (see salt sampling results). Conversely to Huinink et al. (2004), in our
515 study site this area is located at the base and not in the upper parts of the tafoni. This
516 might be due to the specific topographic situation at Tafraoute. In this case, we
517 assume that under the rock tor at our main study site a lens of high soil moisture
518 develops (Fig. 12), a situation which may be different under isolated blocks or in
519 higher positions of a rock wall.

520

521 Figure 12: a) Salt concentrations and moisture gradients according to the
522 measurements; b) supposed distribution of saturated rock; c) supposed migration
523 paths of salts.

524 The model outlined in Figure 12 is based on our findings from Tafraoute. One of the
525 core questions is if water and salts, respectively, derive from the outside (fog, rain,
526 dew, aeolian salt deposition) or from the inside (groundwater body) of the rock. We
527 assume two possible pathways of salt enrichment. (1) Water (with salts) infiltrates
528 from the top of the tor (red arrow) and from the relatively flat surrounding (blue arrow)
529 and forms a body of +/- saturated rock under and within the tor. Due to evaporation
530 and vapor pressure gradients, capillary water is sucked to the surface and salts are
531 precipitated near the surface. The main area of salt enrichment at site 1 is the basal
532 area of the tafone due to the proximity to the saturated zone (primary path). (2) Salts
533 may be also deposited with aeolian dust. On smooth rock faces without tafoni, large
534 portions of these salts are probably washed off while inside the tafoni they remain at
535 the rock surface, or are dissolved during dewfall events and infiltrate into the
536 outermost centimeters of rock (secondary path). Both outlined mechanisms lead to
537 salt concentration in sheltered places and near the base of the rock. This model
538 contradicts the work of Bradley et al. (1978) and the model of Huinink et al. (2004)
539 both of which hypothesized that salts (as well as moisture) should be primarily found
540 in the upper, protected areas of tafoni while the lower parts of the tafoni are probably
541 more exposed to wind, rain and radiation. A reason for the unexpectedly high salt
542 and moisture content in the lower parts of the investigated tafoni at Tafraoute could
543 be that these areas receive a higher input of atmospheric salts. However, if this was
544 the case a markedly higher amount of salt would have to be expected outside of the
545 tafoni which is not the case (with the notable exception of the roof of tafone 3, see
546 below). Thus, for the inside of the tafoni it is more likely that the salts originate from a
547 water body (or area of higher humidity) inside the rock from where they are
548 transported by capillary transport towards the surface. This would mean that tafoni in

549 comparable settings mainly develop near the base of boulders and tors and up to the
550 assumed level of capillary rise which is, in fact, often the case.

551 The salt concentration at the top of the boulder at site 3 shows a significant increase
552 in salt concentration with depth (Fig. 11, dashed line) and thus differs from the
553 profiles inside the tafoni at sites 1 and 3. A reason for this could be the combination
554 of rain and rapid dehydration caused by the high direct radiation. Due to fast drying
555 after rain, atmospheric salts crystallize at a certain depth. During subsequent rain
556 events the salts are successively transported to greater depths (Fig. 12, red arrow).
557 This pathway of salt displacement would explain the development of Tafoni in higher
558 areas of tors and their growth upwards. This assumption is, however, supported only
559 by one measurement and is therefore speculative.

560 *Implications for salt weathering*

561 Textbook concepts of salt weathering assume that damage is induced by (i)
562 crystallization pressure (Correns, 1949; Scherer, 1999), (ii) stresses induced by
563 crystal hydration (Mortensen, 1933; Winkler and Wilhelm, 1970) and (iii) a differential
564 thermal expansion of salts (Cooke and Smalley, 1968; Charola, 2000). The borehole
565 humidity data derived from the iButtons can be used to underpin these assumptions.
566 With high probability, the dominant salt at our study sites is sodium sulfate which
567 occurs in nature in two varieties: The water-free thenardite and the hydrated variety
568 mirabilite. A third metastable variety which might crystallise on cooling to around
569 10°C was reported on by Hall and Hamilton (2008). Assuming that crystallization
570 pressure is the primary source of damage, Rodriguez-Navarro et al. (2000) argued
571 that precipitation of thenardite rather than mirabilite may be responsible for damage
572 from sodium sulfate, particularly in situations of constant capillary rise.

Figure 13: Phase diagram for sodium sulfate. The continuous lines indicate the limits between the stable phases. The discontinuos line corresponds to a solution in metastabile eqilibrium with respect to thenardite and supersaturated with respect to mirabilite (Tsui et. al, 2003). The grey rectangles (Site1 west) indicate the measured T/H data at 50 and 3 cm depth from 21/2/14 to 23/2/14; the rectangles (Site 1 east) indicate the measured T/H data at 50,20 and 3cm depth from 14/2/14 to 24/2/14, respectively.

As Figure 13 shows, the results of our micro-climatic measurements suggest that due to higher humidities found in the pores, sodium sulfate at a depth of 50 cm should occur in dissolved form (or supersaturated with respect to mirabilite). Just below the surface (3 cm), however, the anhydritic thenardite should prevail. Due to the short measurement period the conclusions are speculative; yet it can be assumed that the mirabilite-thenardite transition frequently occurs at this depth range, either by the capillary transport towards the surface and crystallization, or because of changing weather conditions when the surface is wetted or the drying front propagates deeper into the rock in summer. These patterns were also found at the east side of site 1 and at site 5 and 6 (not displayed).

CONCLUSIONS

To sum up, the following conclusions can be drawn from the measurements presented here:

- The combination of high-resolution temperature, moisture and salt measurements enables valuable insights into tafoni formation at our study site in Tafraoute, Morocco. The results derived from very different techniques (IR,

T and H sensors, ERT, hand held moisture meters, drill dust sampling) mutually support one another.

- Our results confirm that moisture and salt concentration are elevated inside tafoni as compared to the surrounding rock.
- A clear correlation was found between moisture and salt contents. Within a tafone, areas of higher humidity also display increased salt concentration near the surface. ERT reacts to both parameters; the least resistive areas are those with high levels of both moisture and salts.
- Our measurements clearly show a significant accumulation of salts close to the rock surface in tafoni, but not on the surrounding rock surfaces. These findings appear to be consistent with the model of Huinink et al. (2004) which predicts enhanced salt deposition in zones of low drying rates.
- Salts and moisture at our sites were concentrated near the base of tafoni which has, to our knowledge, not been reported in the literature before. We assume that the reason is a saturated pore water body around the base of rock tors which might be common in most places other than highly free-standing boulders.
- The measured T/H-values indicate that salts (in this case sodium sulfate) occur in various phases which implies frequent phase changes from thenardite to mirabilite and vice versa.
- Two pathways of salt transport in and around tafoni are assumed based on the data: Infiltration with rainfall on the top and around tors and boulders, and capillary rise from saturated pore water bodies to the surface. Direct dry deposition is probably of subordinate importance.

ACKNOWLEDGEMENTES

This study was supported by travel stipends of the University of Graz provided for S. Fruhmann and H. Schnepfleitner. Warmest thanks to Dr Mona Edwards and Krystyna Krzyżewska who did the IC work.

REFERENCES

- Angelopoulos MC, Pollard WH, Couture NJ. 2013. The application of CCR and GPR to characterize ground ice conditions at Parsons Lake, Northwest Territories. *Cold Regions Science and Technology* **85**: 22-33.
- Barbey P, Oberli F, Burg J-P, Nachit H, Pons J, Meier M. 2004. The Palaeoproterozoic in western Anti-Atlas (Morocco): a clarification. *Journal of African Earth Sciences* **39**: 239-245.
- Benziane F. 2007. Lithostratigraphie et évolution géodynamique de l'anti-Atlas (Maroc) du paléoprotérozoïque au néoprotérozoïque: exemples de la boutonnière de Tagragra Tata et du Jebel Saghro. Doctoral thesis, Université Savoie, France.
- Bradley WC, Hutton JT, Twidale CR. 1978. Role of Salts in Development of Granitic Tafoni, South Australia. *The Journal of Geology* **86**(5), 647-654.
- Brandmeier M, Kuhlemann J, Krumrei I, Kappler A, Kubik PW. 2011. New challenges for tafoni research: A new approach to understand processes and weathering rates. *Earth Surface Processes and Landforms* **36**: 839-852.
- Boelhouwers J, Jonsson M. 2013. Critical Assessment of the 2°C min^{-1} Threshold for Thermal Stress Weathering. *Geografiska Annaler: Series A, Physical Geography* **95**(4): 285–293
- Budzier H, Gerlach G. 2010. Thermische Infrarot Sensoren. Wiley-VCH: Weinheim
- Campbell SW. 1999. Chemical weathering associated with tafoni at Papago Park, Central Arizona. *Earth Surface Processes and Landforms* **24**: 271-278.
- Charola AE. 2000. Salts in the deterioration of porous materials: An overview. *Journal of the American Institute for Conservation* **39**: 327-343.
- Cooke RU, Smalley IJ. 1968. Salt Weathering in Deserts. *Nature* **220**: 1226-1227.

650 – Correns C. W. 1949. Einführung in die Mineralogie (Kristallographie und
651 Petrologie), Springer-Verlag, Berlin-Göttingen-Heidelberg. 414 S., 405 Abb., 1
652 Tafel. Geh. DM 38.—, geb. DM 41.60
653 – Defant A, Defant F. 1958. Physikalische Dynamik der Atmosphäre. Akademische
654 Verlagsgesellschaft: Frankfurt.
655 – Dionisio A, Martinho E, Grangeia C, Almedia F. 2013. Examples of the Use of
656 Non-Invasive Techniques for the Evaluation of Stone Decay in Portugal. *Key*
657 *Engineering Materials* **548**: 239–246.
658 – Doehne E. 2002. Salt weathering: a selective review. In: Natural Stone,
659 Weathering Phenomena, Conservation Strategies and Case Studies. *Geological*
660 *Society Special Publications* **205**: 51–64.
661 – Dorn RI, Gordon SJ, Krinsley D, Langworthy K. 2013. Nanoscale: Mineral
662 Weathering Boundary. In: Treatise on geomorphology. Oxford: Academic.
663 – Eklund JA, Zhang H, Viles HA, Curteis T. 2013. Using Handheld Moisture Meters
664 on Limestone: Factors Affecting Performance and Guidelines for Best Practice.
665 *International Journal of Architectural Heritage* **7**: 207-224.
666 – Franzen C, Mirwald PW. 2009. Moisture sorption behaviour of salt mixtures in
667 porous stone. *Geochemistry* **69**: 91–98.
668 – French HM, Guglielmin M. 2000. Cryogenic weathering of granite, northern
669 Victoria land, Antarctica. *Permafrost and Periglacial Processes* **11**: 305-314.
670 – Goudie AS. 1977. Sodium sulphate weathering and the disintegration of Mohenjo-
671 Daro, Pakistan. *Earth surface processes* **2**(1): 75-86.
672 – Goudie AS, Viles HA. 1997. Salt Weathering Hazards. Wiley: Chichester, New
673 York.
674 – Gaussorgues, G.; Chomet, S. 1993: Infrared Thermography. Springer Verlag, ISBN
675 0412479001
676 – Gruner, K. 2004: Grundlagen der berührungslosen Temperaturmessung
677 „Strahlungsthermometrie“. Revision B1. 12/2004. Raytek Europazentrale,
678 RaytekGmbH, Berlin,32.
679 – Hall C, Hamilton A. 2008. The heptahydrate of sodium sulfate: Does it have a role
680 in terrestrial and planetary geochemistry? *Icarus* **198**: 277-279.

- Hall K, André MF. 2001. New insights into rock weathering from high-frequency rock temperature data: An Antarctic study of weathering by thermal stress. *Geomorphology* **41**: 23-35.
- Hall K. 1986. Rock Moisture Content in the Field and the Laboratory and its Relationship to Mechanical Weathering Studies. *Earth Surface Processes and Landforms* **11**: 131-142.
- Hall K. 1991. Rock moisture data from the Juneau Icefield (Alaska) and its significance for mechanical weathering studies. *Permafrost and Periglacial Processes* **2**: 321-330.
- Hall K, Meiklejohn I, Arocena J. 2007. The thermal responses of rock art pigments: Implications for rock art weathering in southern Africa. *Geomorphology* **91**: 132–145
- Hassenforder B. 1985. Les mylonites de la zone de faille ductile pan-africaine des Ameln (Kerdous, Anti-Atlas occidental, Maroc). Une analyse pétrostructurale de la déformation. *Sciences géologique Strasbourg* **38**: 215-226.
- Hassenforder B. 1987. La tectonique panafricaine et varisque de l'Anti-Atlas dans le massif du Kerdous (Maroc). Doctoral thesis, University of Strasbourg.
- Hilbich C, Marescot L, Hauck C, Loke MH, Mäusbacher R. 2009. Applicability of electrical resistivity tomography monitoring to coarse blocky and ice-rich permafrost landforms. *Permafrost and Periglacial Processes* **20**(3): 269-284
- Huinink HP, Pel L, Kopinga K. 2004. Simulating the growth of Tafoni. Earth *Surface Processes and Landforms* **29**: 1225–1233.
- James WL. 1963. Electric moisture meters for wood. Madison, WI: U.S. Forest Service.
- Kearey P, Brooks M, Hill I. 2002. An introduction to geophysical exploration. Blackwell Science: Malden.
- Krus M. 1995. Feuchtetransport- und Speicherkoeffizienten poröser mineralischer Baustoffe. Theoretische Grundlagen und neue Messtechniken. Doctoral thesis, Universität Stuttgart.
- Marescot L, Loke MH, Chapellier D, Delaloye R, Lambiel C, Reynard E. 2003. Assessing reliability of 2D resistivity imaging in mountain permafrost studies using the depth of investigation index method. *Near Surface Geophysics* **1**(2): 57-67.
- Maroc Météo. 2011. Climat des Villes du Maroc. http://www.marocmeteo.ma (accessed 15/06/2014)

715 – Martinho E, Alegria F, Dionisio A, Grangeia C, Almeida F. 2012. 3D-resistivity
716 imaging and distribution of water soluble salts in Portuguese Renaissance stone
717 bas-reliefs. *Engineering Geology* **141-142**: 33–44.
718 – Materialarchiv. 2014. http://www.materialarchiv.ch/detail/43#/detail/43/granit
719 (accessed 05/03/2015)
720 – Matsukura Y, Takahashi K. 2000. A new technique for rapid and non-destructive
721 measurement of rock-surface moisture content; preliminary application to
722 weathering studies of sandstone blocks. *Engineering Geology* **55**: 113-120.
723 – Maurício A, Figueiredo C, Aires-Barros L. 2006. Monitoring salt systems in
724 monument stones: comparing two electrochemical methods. In: Proceedings of
725 the International Conference on Heritage, Weathering and Conservation (HWC-
726 2006). Taylor & Francis: London.
727 – McBride EF, Picard MD. 2000. Origin and development of tafoni in Tunnel Spring
728 Tuff, Crystal Peak, Utah, USA. *Earth Surface Processes and Landforms* **25**(8):
729 869-879.
730 – Mellor A, Short J, Kirkby SJ. 1997. Tafoni in the El Chorro area, Andalucia,
731 southern Spain. *Earth Surface Processes and Landforms* **22**: 817-833.
732 – Mol L, Viles HA. 2010. Geoelectric investigations into sandstone moisture
733 regimes: Implications for rock weathering and the deterioration of San Rock Art in
734 the Golden Gate Reserve, South Africa. *Geomorphology* **118**: 280-287.
735 – Mol L, Viles HA. 2012. The role of rock surface hardness and internal moisture in
736 tafoni development in sandstone. *Earth Surface Processes and Landforms* **37**:
737 301-314.
738 – Mortensen H. 1933. Die 'Salzsprengung' und ihre Bedeutung für die regional
739 klimatische Gliederung der Wüsten. *Petermanns Geographische Mitteilungen* **79**:
740 130-135.
741 – Mottershead DN, Pye K. 1994. Tafoni on Coastal Slopes, South Devon, U.K.
742 *Earth Surfaces Processes and Landforms* **19**: 543-563.
743 – Mustoe GE. 1983. Cavernous weathering in the Capitol Reef Desert, Utah. *Earth*
744 *Surface Processes and Landforms* **8**: 517-526.
745 – Oldenburg DW, Li Y. 1999. Estimating depth of investigation in DC resistivity and
746 IP surveys. *Geophysics* **64**(2): 403-416.

747 – Plagge R, Funk M, Scheffler G, Grunewald J. 2006. Experimentelle Bestimmung
748 der hygrischen Sorptionsisotherme und des Feuchtetransportes unter
749 instationären Bedingungen. *Bauphysik* **28**(2): 81–87.
750 – Rodriguez-Navarro C, Doehne E, Sebastian E. 1999: Origins of honeycomb
751 weathering: the role of salts and wind. *Geological Society of America Bulletin* **111**:
752 1250-1255.
753 – Rodriguez-Navarro C, Doehne E, Sebastian E. 2000. How does sodium sulfate
754 crystallize? Implications for the decay and testing of building materials. *Cement*
755 *and concrete research* **30**(10): 1527-1534.
756 – Sass O. 2003. Moisture distribution in rockwalls derived from 2D-resistivity
757 measurements. Geophysical applications in geomorphology, Zeitschrift für
758 Geomorphologie Suppl. **132**: 51–69.
759 – Sass O. 2005. Rock moisture measurements: techniques, results, and
760 implications for weathering. *Earth Surface Processes and Landforms* **30**: 359-374.
761 – Sass O, Viles HA. 2010a. Wetting and drying of masonry walls: 2D-resistivity
762 monitoring of driving rain experiments on historic stonework in Oxford, UK.
763 *Journal of Applied Geophysics* **70**: 72-83.
764 – Sass O, Viles HA. 2010b. 2D resistivity surveys of the moisture contents of
765 historic limestone walls in Oxford, UK: Implications for understanding
766 catastrophic stone deterioration. In: Smith, B.J., Gomez Heras, M., Viles, H.A. and
767 Cassar, J. (eds.): Limestone in the built environment: Present day challenges for
768 preservation of the past. *Geological Society of London Special Publication* **331**:
769 237-249.
770 – Scherer G. 1999. Crystallization in pores: Princeton University, CEE/PMI, Eng.
771 Quad. E-319, Princeton, NJ 08544, USA: Cement and Concrete Research 29
772 (1999) 1347–1358
773 – Schrott, L, Sass O. 2008. Application of field geophysics in geomorphology:
774 Advances and limitations exemplified by case studies. *Geomorphology* **93**: 55-73.
775 – Schuster N, Kolobrodov VG. 2000. Infrarotthermographie. WILEY-VCH:
776 Weinheim.
777 – Service Géologique du Maroc (ed.). 1985. Carte géologique du Maroc. Échelle:
778 1/1000000, Rabat.
779 – Shannon HR, Sigda JM, Van Dam RL, Hendrickx JMH, McLemore VT. 2005.
780 Thermal Camera Imaging of Rock Piles at the Questa Molybdenum Mine, Questa,

781 New Mexico. - In: Proceedings of a Joint Conference of American Society of
782 Mining and Reclamation (ASMR) 22nd Annual National Conference.
783 – Skaar C. 1988. Wood–water relations. Springer-Verlag: Berlin.
784 – Soulaimani A, Piqué A. 2004. The Tasrirt structure (Kerdous inlier, Western Anti-
785 Atlas, Morocco): a late Pan-African transtensive dome. *Journal of African Earth*
786 *Sciences* **39**(3): 247-255.
787 – Strini A, Guglielmin M, Hall K. 2008. Tafoni development in a cryotic environment:
788 an example from Northern Victoria Land, Antarctica. *Earth Surface Processes and*
789 *Landforms* **33**: 1502–1519.
790 – Sumner PD, Hall KJ, van Rooy JL, Meiklejohn KI. 2009. Rock weathering on the
791 eastern mountains of Africa: Review and insight from case studies. *Journal of*
792 *African Earth Sciences* **55**: 236-244.
793 – Testo AG (ed.). 2006. Leitfaden zur Infrarot-Messtechnik. http://www.testo.com
794 (accessed 06/2011).
795 – Teza G, Marcato G, Castelli E, Galgaro A. 2011. IRTROCK: A MATLAB toolbox
796 for contactless recognition of surface and shallow weakness of a rock cliff by
797 infrared thermography. *Computer & Geosciences* **45**: 109-118.
798 – Tsui N, Flatt RJ, Scherer GW. 2003. Crystallization damage by sodium sulphate.
799 *Journal of Cultural Heritage* **4**: 109-115.
800 – Turkington AV, Phillips JD. 2004. Cavernous weathering, dynamical instability and
801 self-organization. *Earth Surface Processes and Landforms* **29**: 665-675.
802 – Turkington AV, Martin E, Viles HA, Smith BJ. 2003. Surface change and decay of
803 sandstone samples exposed to a polluted urban atmosphere over a six-year
804 period: Belfast, Northern Ireland. *Building and Environment* **38**: 1205-1216.
805 – Turkington, AV, Paradise TR. 2005. Sandstone weathering: A century of research
806 and innovation. *Geomorphology* **67**(1): 229-253.
807 – Viles HA, Goudie AS. 1992. Weathering of limestone columns from the
808 Weymouth seafront, England. In: Proceedings of the 7th International Congress
809 on Deterioration and Conservation of Stone, Lisbon, June 1992.
810 – Winkler EM, Wilhelm EJ. 1970. Salt burst by hydration pressures in architectural
811 stone in urban atmosphere. *Geological society of America bulletin*, **81**(2): 567-
812 572.
813

Table

Table 2

	iButtons (surface)	iButtons (temperature profiles, 3 depths)	iButtons (moisture profiles, 2 depths)	IR Cam 24-hr monitor.	moisture meter grids	ERT profiles	Sampling drillholes
site1W	**1**	**1**	**1**	**1**	**2**	**10***	**4**
site 1E	-	1	**1**	1	**1**	1	1
site 1S	1	1	1	1	-	1	-
site 1N	-	1	1	-	-	-	-
site 2W	-	1	-	-	1	1	-
site 2E	-	-	-	-	-	1	1
site 3	-	-	-	-	**2***	**3****	**2**
site 4	-	-	-	-	1	**2****	-
site 5	-	1	1	-	-	-	-
site 6	-	1	1	-	-	-	-

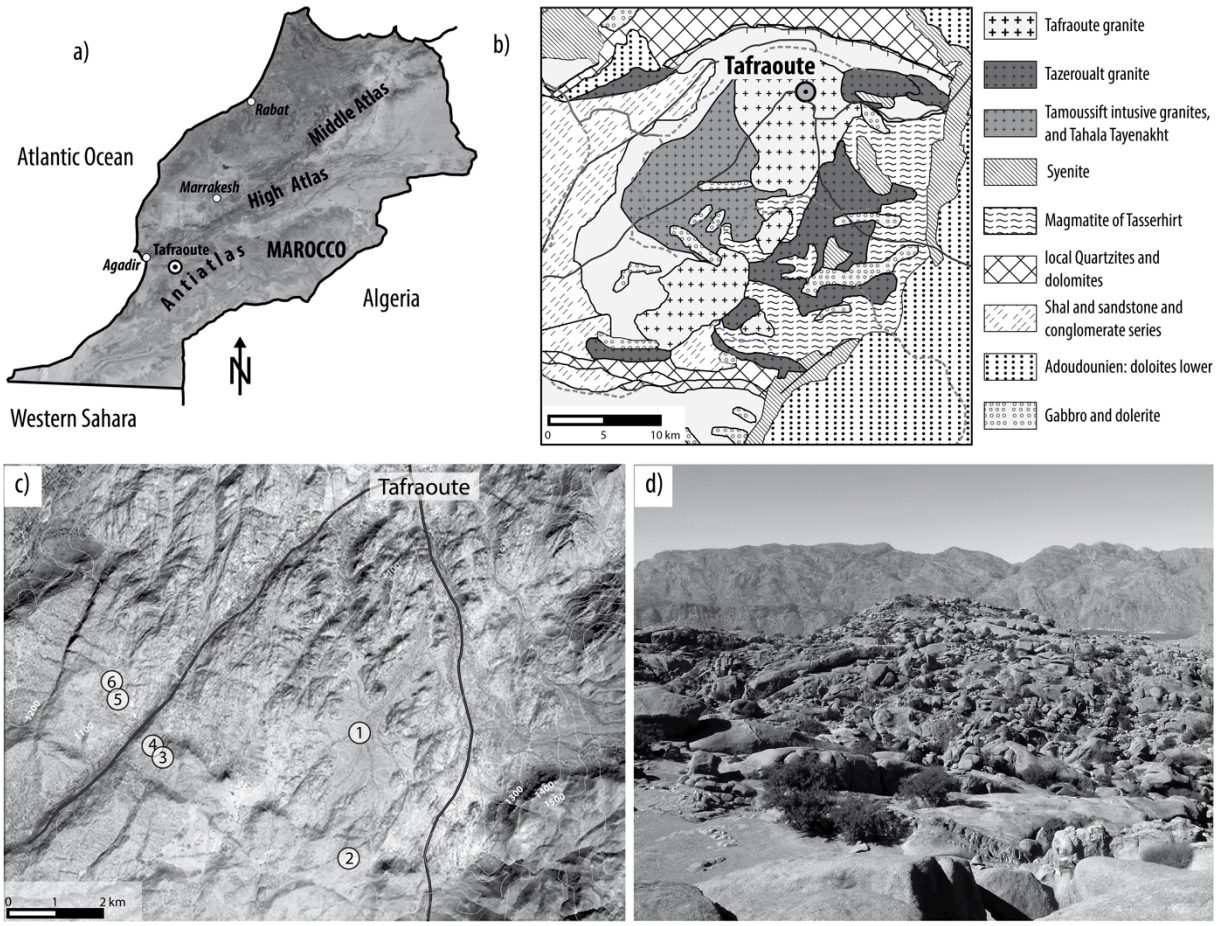

827

828

829 Figure 1 Overview of the study area. (a) location; (b) simplified geological map (taken
830 from Service Géologique du Maroc, 1985); (c) location of the investigated sites in the
831 study area; (d): impression of the granite landscape (taken from site 1 looking north).

832

833

834

835

836

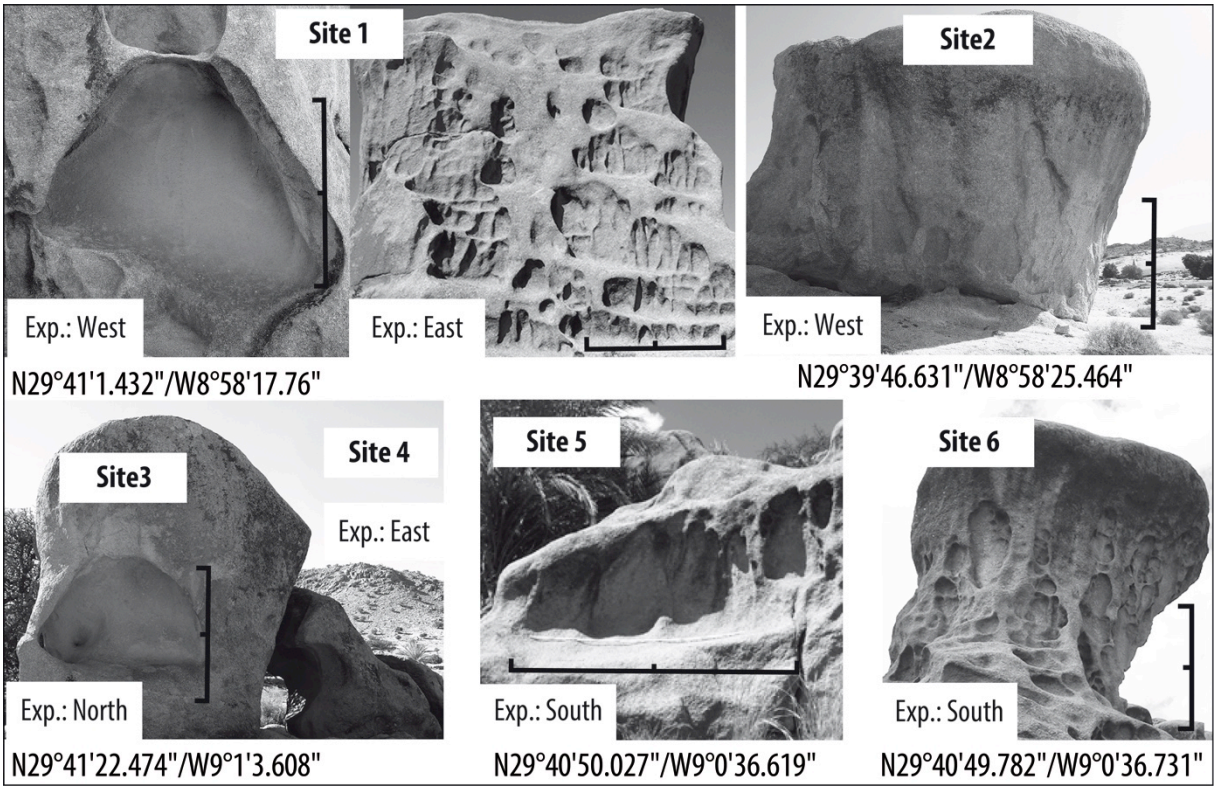

Figure 2 Representation of the different study sites; the black bar denotes 2 m.

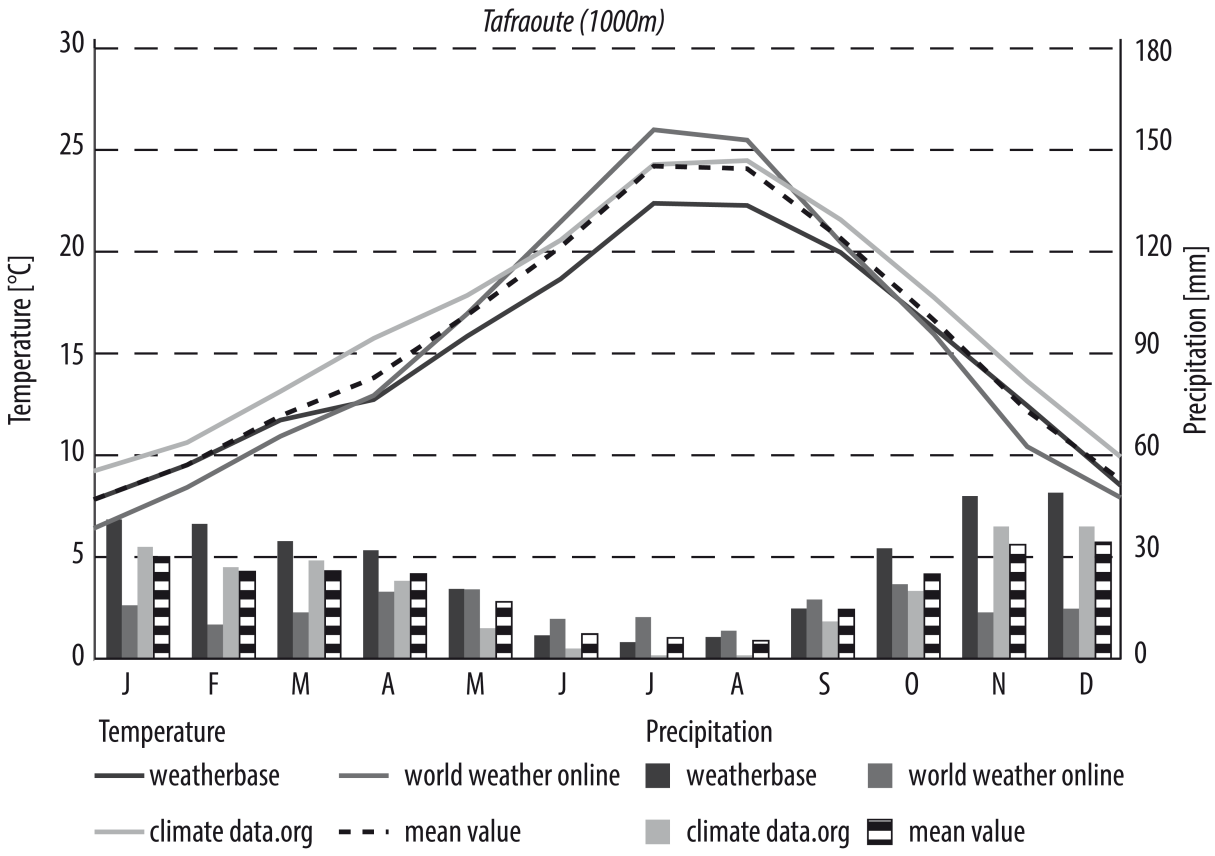

849

850

851 Figure 3 Climate in Tafraoute as derived from different internet sources
852 (http://www.weatherbase.com/, http://www.worldweatheronline.com, ttp://en.climate-
853 data.org).

854

855

856

857

858

859

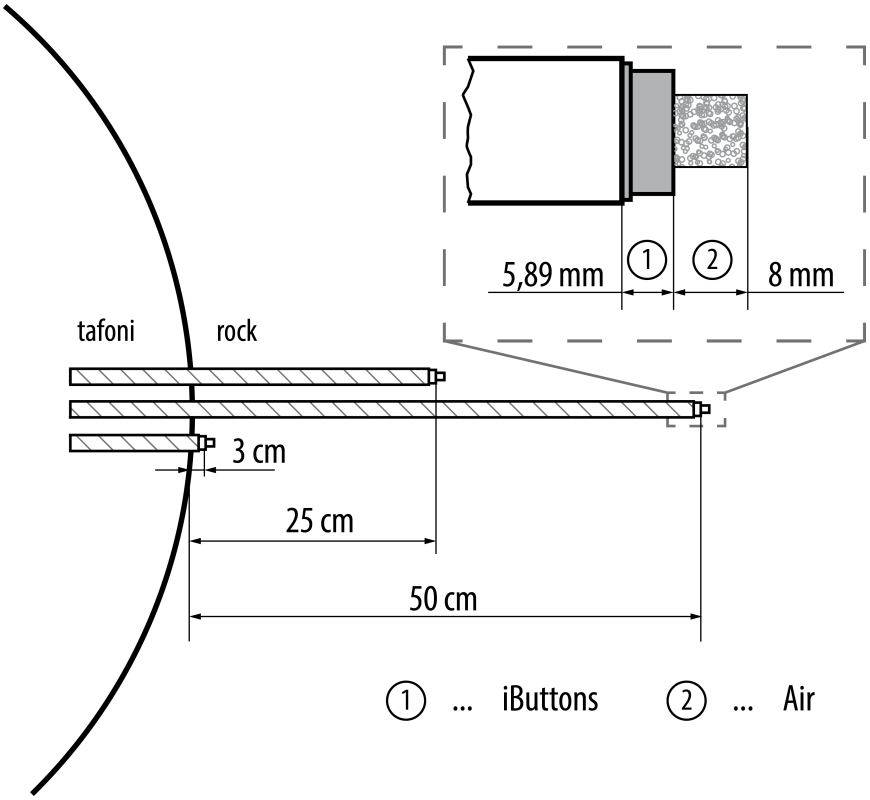

Figure 4 Setup for temperature and relative humidity measurements at different depths. Hatching: wooden rod, gray: iButton.

872

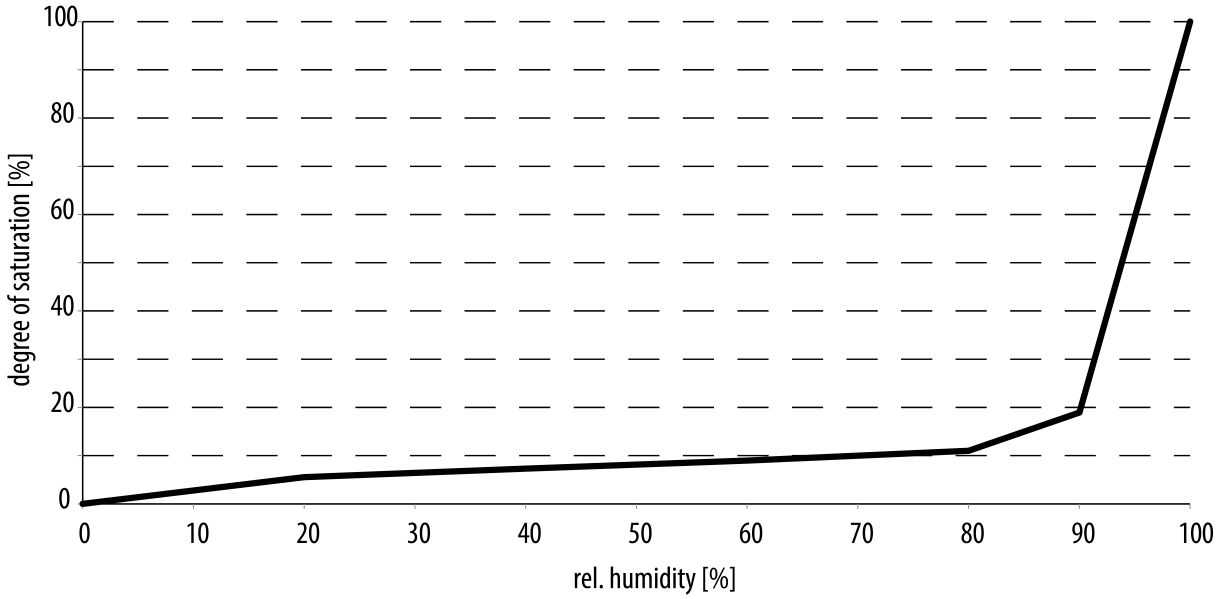

873

874

875 Figure 5 Sorption isotherm of the Tafraoute granite as derived from lab
876 measurements.

877

878

879

880

881

882

883

884

885

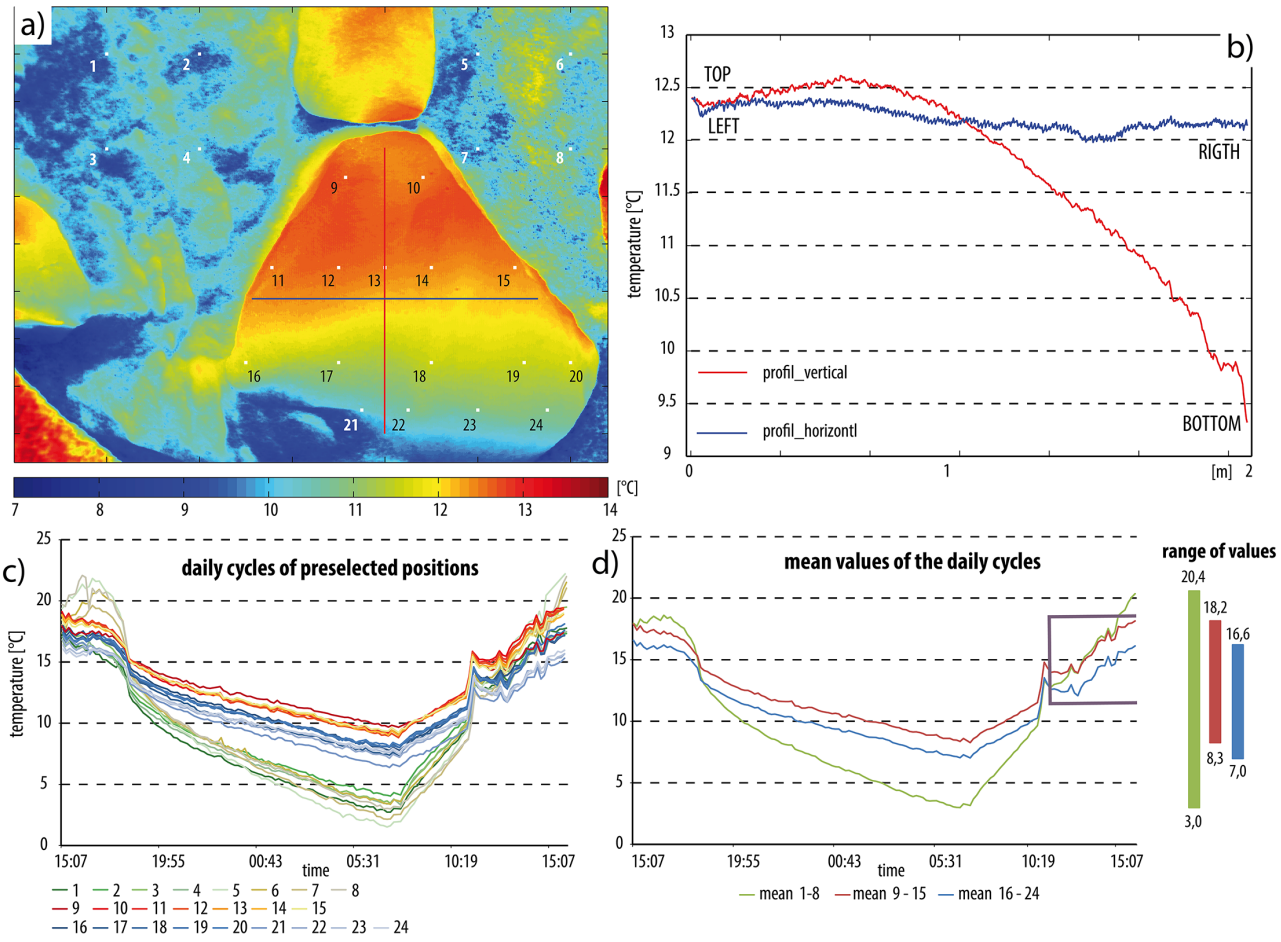

Figure 6 Results of the infrared measurments. (a) Average of the 24 h measurement (dots mark the positions for which the temperature fluctuations were analysed); (b) horizontal and vertical temperature profile (24 h mean); (c) daily temperature cycle at defined points; (d) averaged temperature cycles for certain areas (see text).

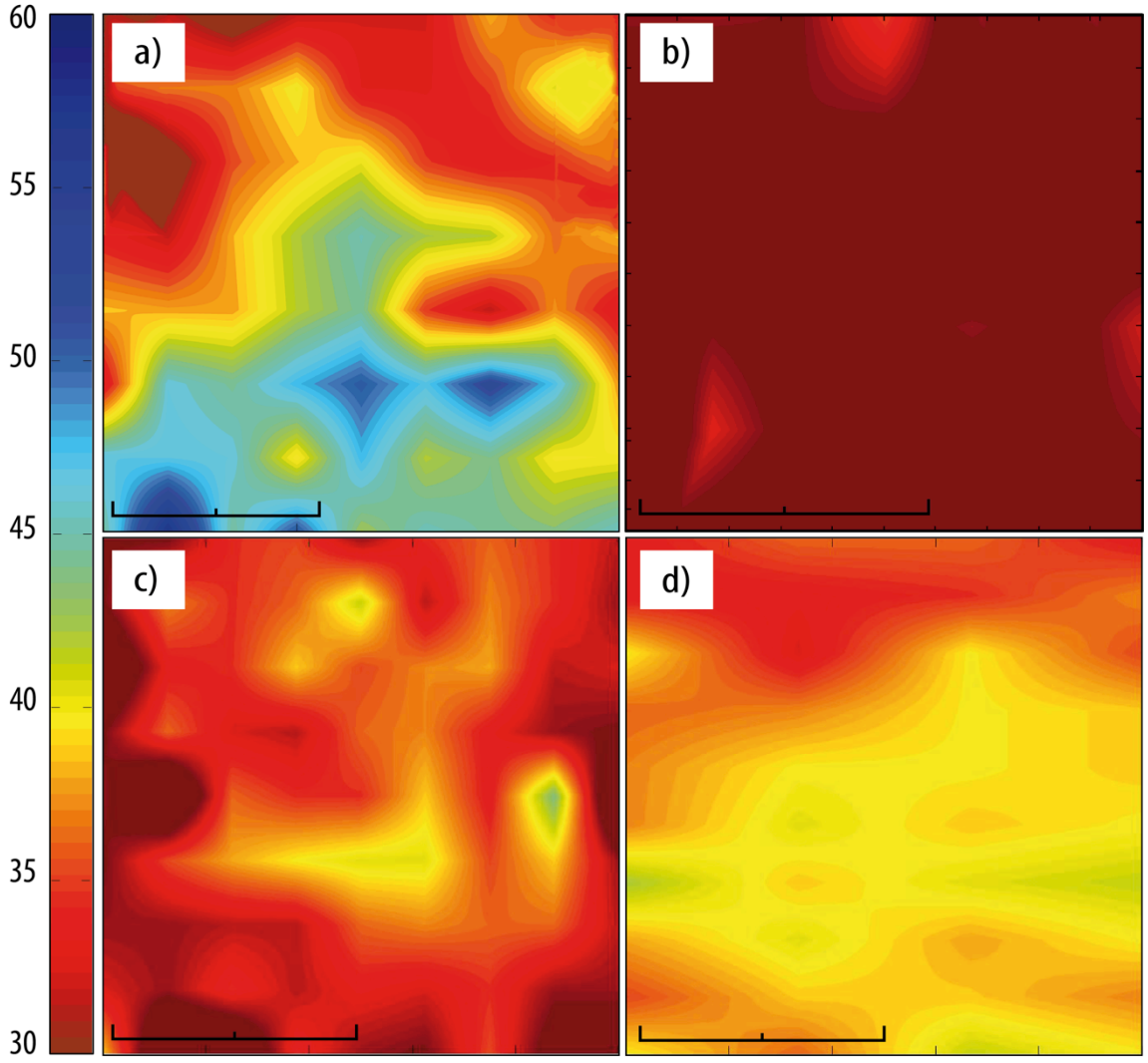

Figure 7 Results of the moisture meter measurements. (a) site 1 (west), inside the tafone; (b) site 1 (west), outside of the tafone; (c) site 1 (east), yellow-green patches correspond to small, shallow tafone; (d) inside the tafone at site 3. Relative readings from 0 (dry) to 100 (wet); the black bar denotes 2 m.

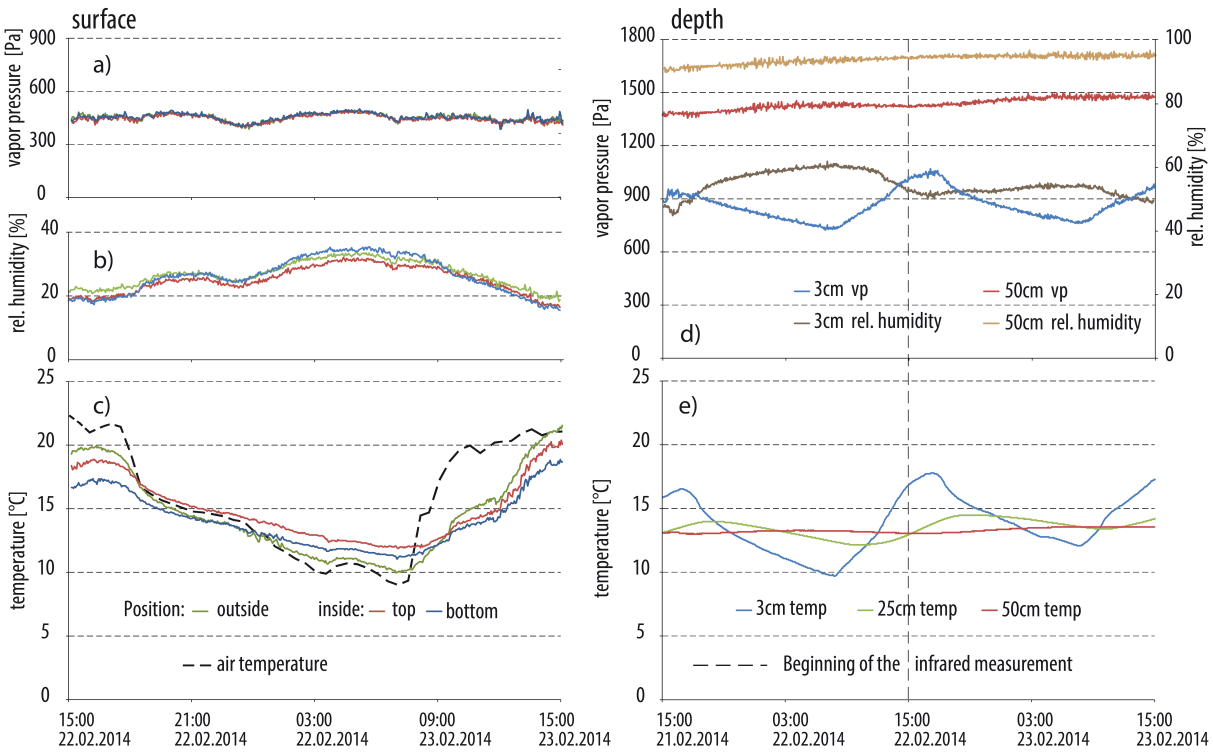

906

907

908 Figure 8 Results of iButtons measurement at site1 (west).

909

910

911

912

913

914

915

916

917

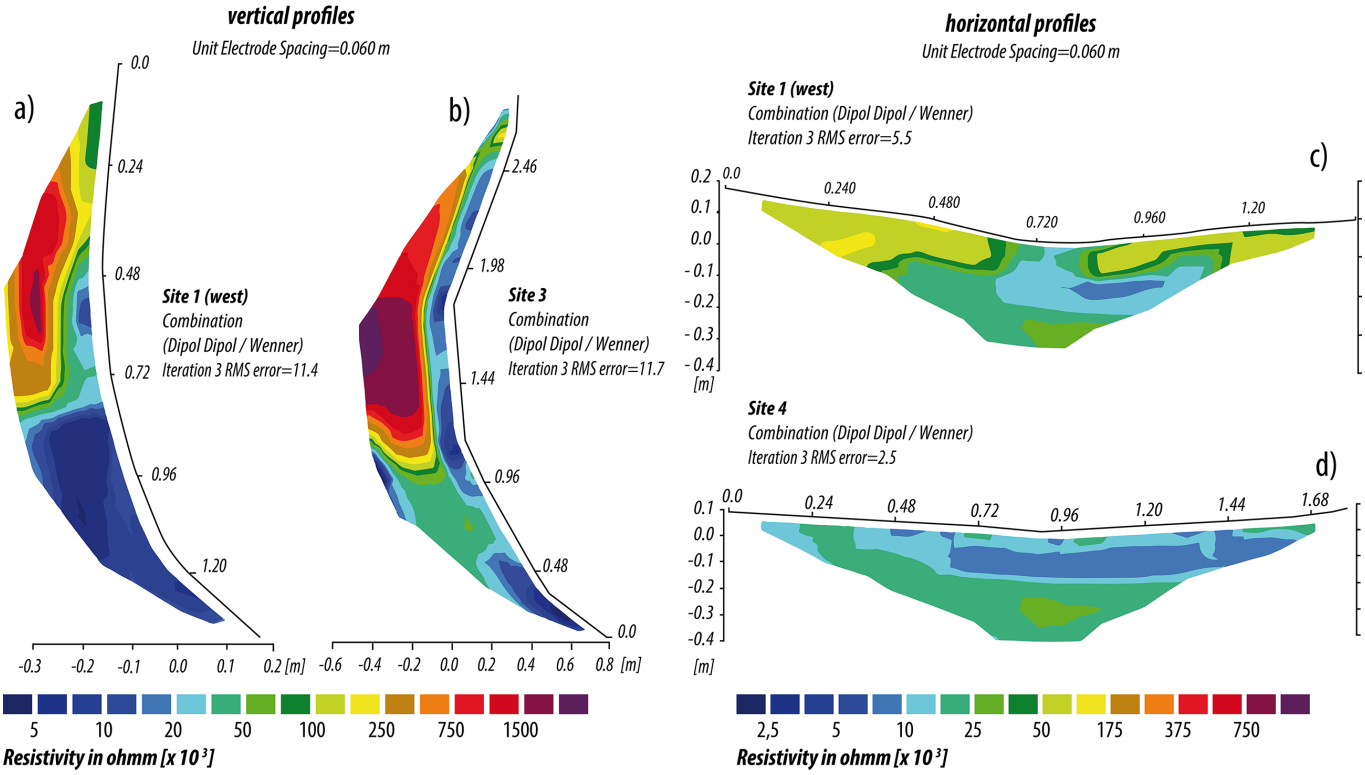

Figure 9 Results of ERT measurement at site 1 west (a), (c), site 3 (b) and site 4 (d). Each profile is combined from Wenner and dipole–dipole measurements; unit electrode spacing is 6 cm.

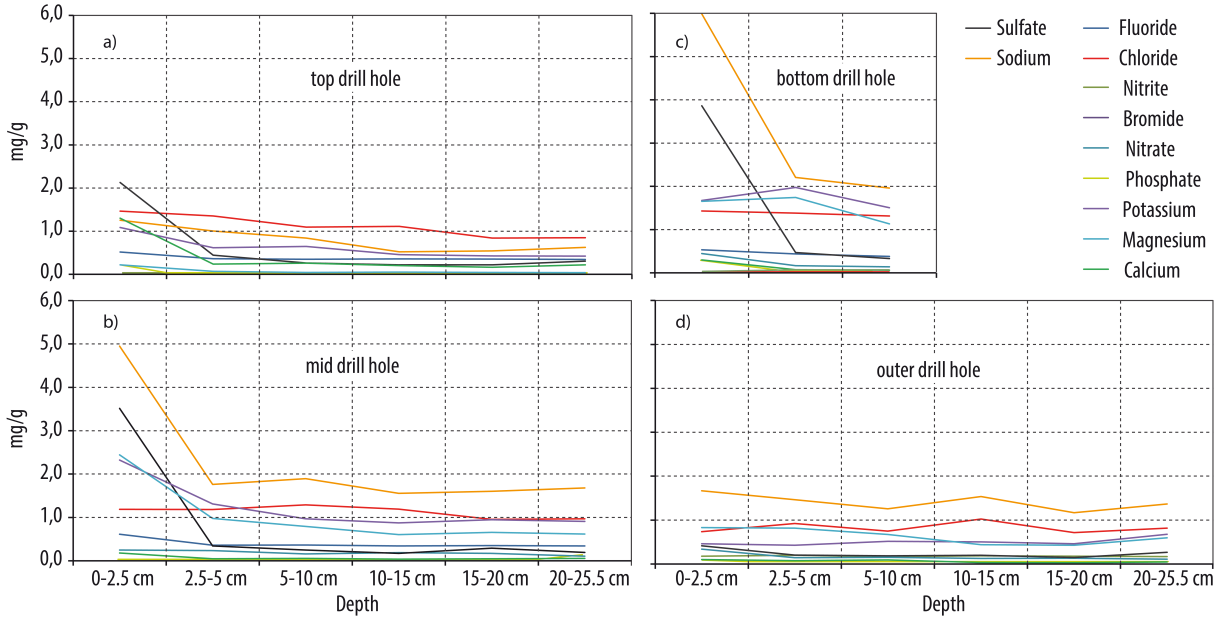

930

931

932 Figure 10 Concentrations of major ions in rock powder from different depths

933 collected from the drillholes of site 1 (west).

934

935

936

937

938

939

940

941

942

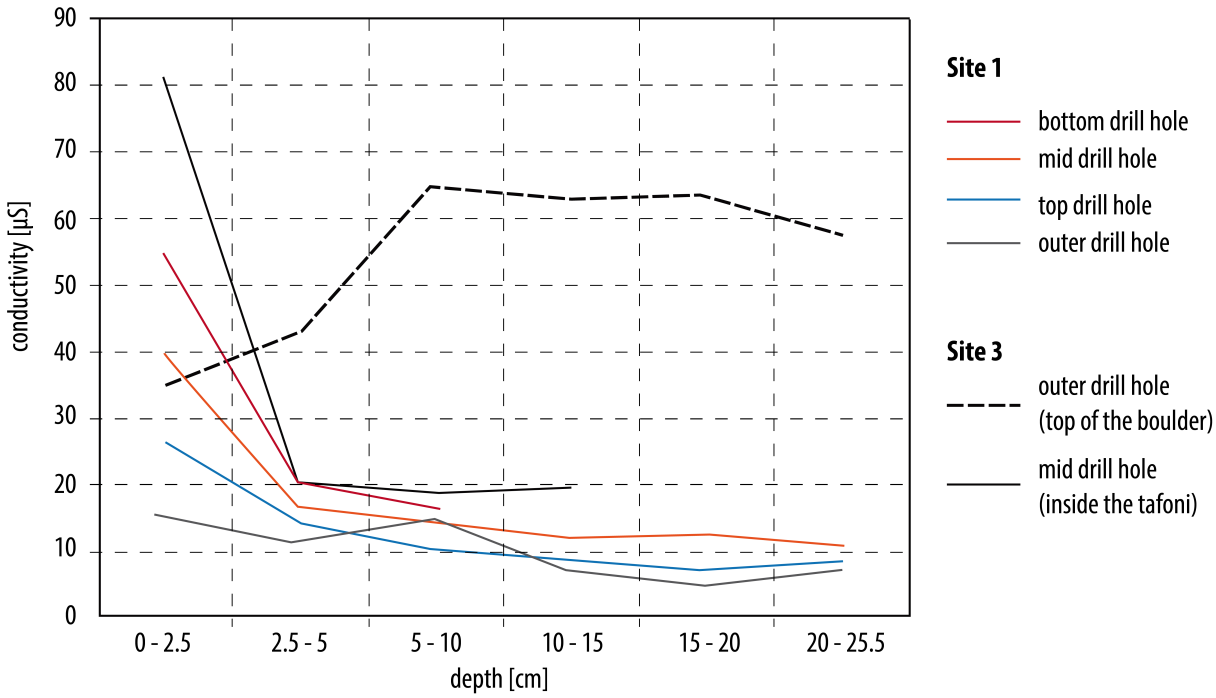

Figure 11 Conductivity values from rock powder from different depths collected from the drillholes in site 1 and site 3.

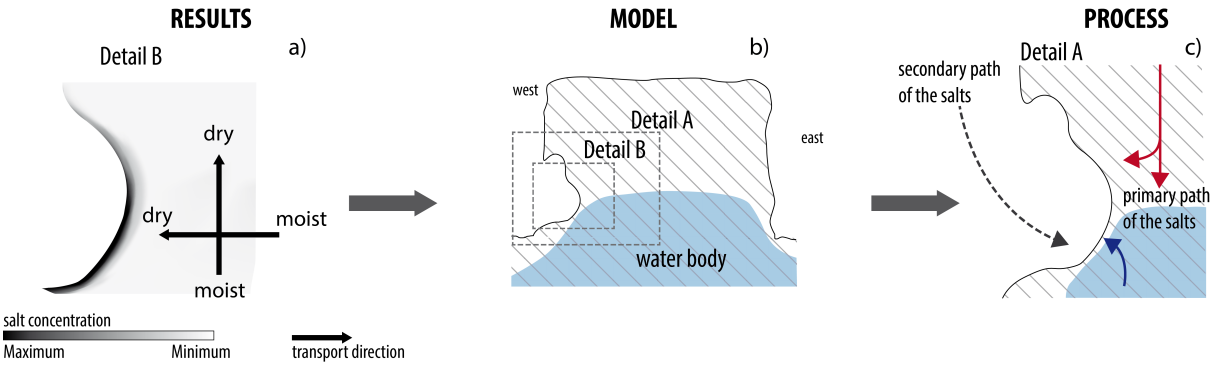

Figure 12 (a) Salt concentrations and moisture gradients according to the measurements; (b) supposed distribution of saturated rock; (c) supposed migration paths of salts.

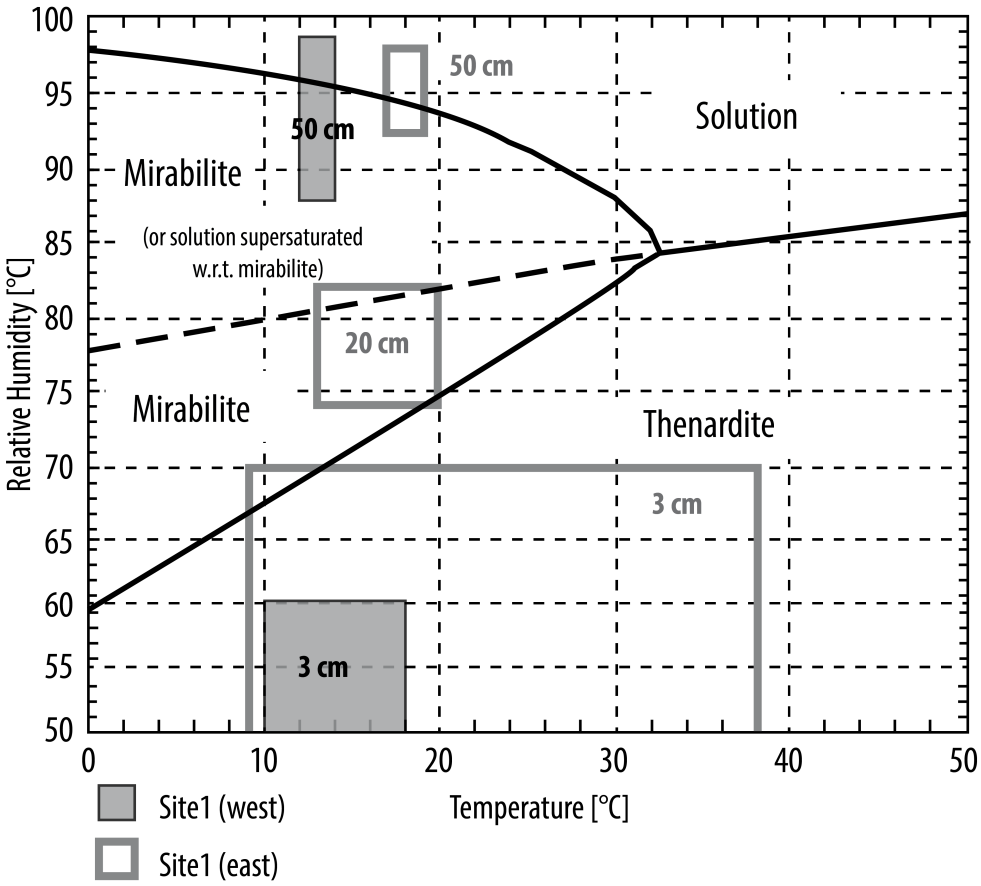

Figure 13 Phase diagram for sodium sulfate. The continuous lines indicate the limits between the stable phases. The discontinuous line corresponds to a solution in metastabile eqilibrium with respect to thenardite and supersaturated with respect to mirabilite (Tsui *et al.,* 2003). The grey rectangles (site1 west) indicate the measured T/H data at 50 and 3 cm depth from 21/2/14 to 23/2/14; the rectangles (site 1 east) indicate the measured T/H data at 50, 20 and 3 cm depth from 14/2/14 to 24/2/14, respectively.